Journal of Solid State Chemistry 182 (2009) 1964–1971

Contents lists available at ScienceDirect

Journal of Solid State Chemistry

journal homepage: www.elsevier.com/locate/jssc

The electronic structures of vanadate salts: Cation substitution as a tool for band gap manipulation

Michelle R. Dolgos, Alexandra M. Paraskos, Matthew W. Stoltzfus, Samantha C. Yarnell, Patrick M. Woodward *

Ohio State University, Department of Chemistry, 100 West 18th Avenue, Columbus, OH 43210, USA

ARTICLE INFO

Article history:
Received 18 September 2008
Received in revised form
29 March 2009
Accepted 5 April 2009
Available online 8 May 2009

Keywords:
Pigments
Photocatalyst
Electronic structure
Charge transfer
Vanadates

ABSTRACT

The electronic structures of six ternary metal oxides containing isolated vanadate ions, $Ba_3(VO_4)_2$, $Pb_3(VO_4)_2$, YVO_4, $BiVO_4$, $CeVO_4$ and Ag_3VO_4 were studied using diffuse reflectance spectroscopy and electronic structure calculations. While the electronic structure near the Fermi level originates largely from the molecular orbitals of the vanadate ion, both experiment and theory show that the cation can strongly influence these electronic states. The observation that $Ba_3(VO_4)_2$ and YVO_4 have similar band gaps, both 3.8 eV, shows that cations with a noble gas configuration have little impact on the electronic structure. Band structure calculations support this hypothesis. In $Pb_3(VO_4)_2$ and $BiVO_4$ the band gap is reduced by 0.9–1.0 eV through interactions of (a) the filled cation 6*s* orbitals with nonbonding O 2*p* states at the top of the valence band, and (b) overlap of empty 6*p* orbitals with antibonding V 3*d*–O 2*p* states at the bottom of the conduction band. In Ag_3VO_4 mixing between filled Ag 4*d* and O 2*p* states destabilizes states at the top of the valence band leading to a large decrease in the band gap ($E_g = 2.2$ eV). In $CeVO_4$ excitations from partially filled 4*f* orbitals into the conduction band lower the effective band gap to 1.8 eV. In the $Ce_{1-x}Bi_xVO_4$ ($0 \le x \le 0.5$) and $Ce_{1-x}Y_xVO_4$ ($x = 0.1, 0.2$) solid solutions the band gap narrows slightly when Bi^{3+} or Y^{3+} are introduced. The nonlinear response of the band gap to changes in composition is a result of the localized nature of the Ce 4*f* orbitals.

1. Introduction

One of the many challenges facing solid state chemists today is the design of nontoxic inorganic pigments. Pigments are used in a wide range of applications including paints, inks, plastics, rubbers, ceramics, enamels, and glasses [1–5]. Unfortunately, many of the best inorganic pigments contain metals that have an undesirable impact on human health and/or the environment. For example, the majority of traditional yellow and red pigments, including chrome yellow ($PbCrO_4$), red lead (Pb_3O_4), cadmium yellow (CdS), iodine scarlet (HgI_2), and vermillion (HgS), contain toxic elements [6]. In order to pursue a rational approach to the discovery of new pigments it is necessary to understand how composition and crystal structure can be manipulated to control the electronic structure.

For decades $PbCrO_4$ was one of the most widely used yellow pigments, but concerns about the toxicity of both lead and chromate have significantly reduced its use [7,8]. From a chemical point of view, moving from a chromate salt to a vanadate salt is a natural strategy. Unfortunately the charge transfer energy of the colorless VO_4^{3-} ion is larger than that of the yellow CrO_4^{2-} ion. Consequently, many vanadate salts are white. Among the compounds that are an exception to this trend, $BiVO_4$ is particularly notable. The monoclinic, fergusonite form of $BiVO_4$ is a deep yellow compound that compares favorably to $PbCrO_4$ as a pigment [9].

Control of the valence and conduction band positions is not only important for designing pigments, such knowledge is essential to rationally approach the search for new photocatalysts. Photocatalysts can be used to convert solar energy into hydrogen, which makes them of great interest to help meet the growing energy demands of our society [10–14]. They also find application in self-cleaning glass [15] and water purification [16]. TiO_2 is the oldest and still the most widely used photocatalyst [17]. Unfortunately, due to its relatively large band gap ($E_g \sim 3.1$ eV in the anatase form) UV photons are needed to drive the photocatalytic process. Consequently only 4% of the available solar energy can be utilized. A photocatalytic material that relies on the less energetic, but more abundant, visible light could make use of a much larger portion of the solar spectrum [18]. This provides a clear and pressing motivation for discovery of effective photocatalysts with smaller band gaps. Interestingly, $BiVO_4$ is not only of interest as a pigment, but it has also been shown to be an effective visible light photocatalyst [10,11]. Other vanadates,

* Corresponding author. Fax: 1 614 292 0368.
E-mail address: woodward@chemistry.ohio-state.edu (P.M. Woodward).

0022-4596/$ - see front matter © 2009 Elsevier Inc. All rights reserved.
doi:10.1016/j.jssc.2009.04.032

including $InVO_4$ [10,12] and Ag_3VO_4 [13,14], have been studied for their photocatalytic properties as well.

In this study the electronic structures of six different salts containing isolated VO_4^{3-} anions are investigated both experimentally and computationally. The results show that the positions of the valence and/or conduction bands of vanadate salts, and charge transfer salts more generally, can be significantly altered through interactions with cations.

2. Experimental and computational methods

2.1. Synthesis

$Pb_3(VO_4)_2$ and Ag_3VO_4 were prepared by a precipitation route. Appropriate quantities of $Pb(NO_3)_2$(aq) and Na_3VO_4(aq) were dissolved in separate 1 M HNO_3(aq) solutions to prepare 1 M solutions of Pb^{2+} and VO_4^{3-}. A $Pb_3(VO_4)_2$ precipitate was obtained by mixing these solutions in a 3:2 volume ratio. Ag_3VO_4 was prepared by a similar route from 1 M $AgNO_3$(aq) and Na_3VO_4(aq) solutions. In the case of Ag_3VO_4 concentrated ammonium hydroxide was slowly added to the precipitate/supernatant mixture while stirring, until a pH of 14 was achieved. This step helped to eliminate phases containing the pyrovanadate ion, $V_2O_7^{4-}$. For both $Pb_3(VO_4)_2$ and Ag_3VO_4 the precipitates were heated to 400 °C for 8 h to drive off residual water and aid crystallization. $BiVO_4$ in the zircon form was also formed via a coprecipitation route in basic solution as described in detail elsewhere [19]. Special care was taken to filter the precipitate quickly to prevent a phase transition to the monoclinic fergusonite phase.

The preparation of YVO_4 followed similar steps to that of $BiVO_4$. First, stoichiometric amounts of V_2O_5 and $Y_2(CO_3)_3$ were mixed in concentrated HCl and heated to 80 °C. The solution was then titrated with 3 M NH_4OH and 30% H_2O_2 until the pH reached approximately 8 and the solution became a gel. The gel was filtered and dried, resulting in an amorphous solid which was heated to 350 °C for 3 h to obtain polycrystalline YVO_4.

$Ba_3(VO_4)_2$ was synthesized using traditional solid state techniques. Stoichiometric ratios of $BaCO_3$ (Alfa Aesar, 99.99%) and V_2O_5 (Fischer Scientific, 99%) were ground together using an agate mortar and pestle. The resulting mixture was heated at 900 °C for 24 h. Solid solutions of $Ce_{1-x}Bi_xVO_4$ and $Ce_{1-x}Y_xVO_4$ were also synthesized via a solid state route. Stoichiometric ratios of CeO_2 (Aldrich, 99.9%), Bi_2O_3 (Alfa Aesar, 99.5%) and/or Y_2O_3 (Alfa Aesar, 99.9%), and V_2O_5 (Fischer Scientific, 99%) were measured out and ground together using an agate mortar and pestle. The homogenous powders were then heated in air at 800 °C for 12 h.

For all samples the phase purity was confirmed using X-ray powder diffraction (XRPD). XRPD patterns for all compounds synthesized can be found in the supplemental information.

2.2. Diffuse reflectance

The band gap of each polycrystalline material was measured using diffuse reflectance spectroscopy. Reflectance data were collected using a Perkin-Elmer Lambda 20 scanning double-beam spectrometer equipped with a 50 mm Labsphere integrating sphere over the spectral range 200–1100 nm (6.2–1.1 eV). The diffuse reflectance data were then converted to absorbance data using the Kubelka–Munk function

$$F(R) = \frac{(1-R)^2}{2R} = \frac{K}{S}$$

where R represents the reflectance, while K and S correspond to the effective absorption and scattering, respectively [20]. Band gaps were determined from the data by extrapolating the steep portion of the absorption edge to the wavelength/energy where the absorbance is zero [21].

2.3. Computational methods

Electronic band structure calculations were performed using the Stuttgart tight binding, linear muffin tin orbital atomic sphere approximation (TB-LMTO-ASA or LMTO for short) code. LMTO is a self-consistent, density functional theory code, which incorporates scalar-relativistic corrections. Detailed descriptions of the ab-initio calculations are given elsewhere [22,23]. The effects of exchange and correlation were approximated using the Perdew–Wang generalized gradient approximation (GGA) [24].

Band structure calculations were also carried out using the Cambridge Serial Total Energy Package (CASTEP) [25]. CASTEP is a first principles density functional theory code that uses a plane wave basis and pseudopotentials to model the potential felt by the electrons in the core region. The generalized gradient approximation (GGA, Perdew–Wang 91) was used for the exchange and correlation effects [24,26]. An accuracy of 0.1 eV/atom was used for convergence.

Molecular orbital calculations were performed using the Amsterdam density functional (ADF) program, version 2002.03, developed by Te Velde and Baerends [27]. The atomic electronic configurations were described using triple-ζ STO basis functions with frozen core levels. Non-local exchange and correlation effects were treated using the corrections of Perdew and Wang (PW91) [26].

2.4. Structural description

To have a complete discussion of the structure–property relationship of $A_x(VO_4)_y$ compounds it is helpful to briefly review the crystal structures of the compounds in question. While all structures contain isolated VO_4^{3-} groups, the cation environment and site symmetries vary from one compound to the next. All of the structures have been previously reported. Table 1 lists the space groups and metal–oxygen bond lengths.

Barium vanadate, $Ba_3(VO_4)_2$, crystallizes in the $R\bar{3}m$ space group with a structure known as palmierite [28–30]. The vanadium ion sits on a site with C_{3v} site symmetry and the VO_4^{3-} tetrahedra are only slightly distorted from T_d geometry. There are two chemically distinct Ba^{2+} sites, one six coordinate and the other ten coordinate. The structure of $Pb_3(VO_4)_2$ is related to $Ba_3(VO_4)_2$ but the threefold rotoinversion axis is lost as a result of a lone pair distortion on the Pb^{2+} ion. This lowers the space group symmetry to $P2_1/c$ and results in a distortion of the local environments of the lead and to a lesser extent the vanadium cations [31].

YVO_4, $CeVO_4$, and $BiVO_4$ all crystallize with the zircon structure (space group $I4_1/amd$). The zircon structure consists of VO_4^{3-} tetrahedra which share edges with AO_8 dodecahedrons to form chains that run parallel to the c-axis [32]. The vanadium environment is quite symmetric with four equivalent V–O bonds. Each A-site cation (Y^{3+}, Ce^{3+}, Bi^{3+}) has D_{2d} site symmetry and is surrounded by eight oxygen atoms forming an antiprism with two different sets of A–O bonds of almost equal length. It should be noted that the zircon form of $BiVO_4$ is a metastable structure. The most stable polymorph is the monoclinic, fergusonite form, which is a distorted variant of the scheelite structure. The electronic structure of monoclinic $BiVO_4$ has been explored in detail elsewhere [19].

Table 1
Space groups and select bond distances in vanadate salts.

Compound	Space group	V–O bond length (Å)	A–O bond length (Å)	Reference
$Ba_3(VO_4)_2$	$R\bar{3}m$	3×1.695 1×1.697	Ba(1): 6×2.758 Ba(2): 6×2.914 3×2.820 1×2.609	[45]
$Pb_3(VO_4)_2$	$P2_1/c$	1×1.684 1×1.697 1×1.726 1×1.744	2×2.581 2×2.619 2×2.769 2×2.894	[46]
YVO_4	$I4_1/amd$	4×1.717	4×2.290 4×2.432	[47]
$CeVO_4$	$I4_1/amd$	4×1.711	4×2.442 4×2.525	[47]
$BiVO_4$ (zircon)	$I4_1/amd$	4×1.703	4×2.414 4×2.548	[48]
Ag_3VO_4	$C2/c$	2×1.711 2×1.732	Ag(1): 1×2.164 1×2.195 1×2.444 1×2.505 Ag(2): 2×2.369 2×2.373	[13]

Silver vanadate, Ag_3VO_4, crystallizes with $C2/c$ space group symmetry. Its crystal structure has been described as an "anti-sphalerite" structure [33]. The VO_4^{3-} tetrahedra are isolated from each other and slightly distorted. The V^{5+} ions have C_2 site symmetry. The silver ions have two chemically distinct environments, one a distorted square planar arrangement with D_{2h} site symmetry and the other a pseudo see-saw configuration with C_1 site symmetry.

3. Results and discussion

3.1. Diffuse reflectance

The diffuse reflectance spectra of the six ternary metal oxides are shown in Fig. 1. Band gaps are extrapolated from the data as described above and the values are listed in Table 2. $Ba_3(VO_4)_2$ and YVO_4 have large, nearly identical band gaps that fall in the UV region. Consequently both compounds are white powders. $Pb_3(VO_4)_2$ and $BiVO_4$, both of which are pale yellow in color, have band gaps of 2.9 and 2.8 eV, respectively. In each case replacing an electropositive cation with a noble gas configuration (Ba^{2+}, Y^{3+}) with a p-block cation with $6s^26p^0$ electron configuration (Pb^{2+}, Bi^{3+}) leads to a significant decrease in the band gap. The band gap of Ag_3VO_4 is further reduced, to a value of 2.2 eV, giving rise to an orange compound. $CeVO_4$ has smaller band gap still, 1.8 eV, which gives it a dark brown appearance.

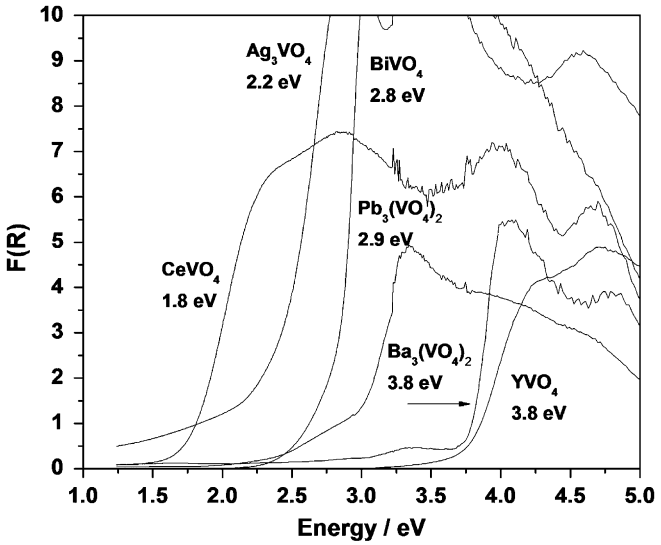

Fig. 1. Diffuse reflectance spectra for select vanadate salts.

3.2. Solid solutions

Solid solutions in the $BiVO_4$–$CeVO_4$ system were prepared to determine the solid solubility range and probe the possibility of using a solid solution approach to systematically vary the color. For the $Ce_{1-x}Bi_xVO_4$ system single phase products were obtained for x values between 0 and 0.5 where the resulting structure was the zircon form. When x values were greater than 0.5, two phase mixtures (zircon and fergusonite) were obtained, in agreement with previous literature reports [34]. The band gap narrows, gradually but linearly, as the bismuth content increases, from 1.8 eV in pure $CeVO_4$ to ~1.5 eV in $Ce_{0.6}Bi_{0.4}VO_4$ and $Ce_{0.5}Bi_{0.5}VO_4$ (Fig. 2). This result is somewhat unexpected given the fact that $BiVO_4$ ($E_g = 2.8$ eV) has a larger band gap than $CeVO_4$. For comparison homogeneous solid solutions were also prepared in the $Ce_{1-x}Y_xVO_4$ system for x values of 0.9, 0.8, 0.2, and 0.1. Just as in the $Ce_{1-x}Bi_xVO_4$ system, replacement of Ce^{3+} leads to a decrease in the band gap as shown in Fig. 3. Interestingly in both cases the band edge becomes sharper as Ce^{3+} is replaced.

3.3. Electronic structure of the vanadate ion

To understand the electronic structure calculations of the ternary metal oxides, we begin with the frontier orbitals of the VO_4^{3-} ion. ADF calculations were performed on this ion and the resulting molecular orbital diagram is shown in Fig. 4 with the corresponding orbital interactions in Fig. 5. The HOMO has t_1 symmetry and is composed of O $2p$ nonbonding orbitals. The

Table 2
Experimental and theoretical band gap values for the $A_x(VO_4)_y$ compounds.

Compound	Exp. band gap (eV)	LMTO calc. band gap (eV)	CASTEP calc. band gap (eV)	Lit. band gap (eV)
$Ba_3(VO_4)_2$	3.8	3.3	3.6	–
$Pb_3(VO_4)_2$	2.9	2.6	2.8	–
YVO_4	3.8	3.0	3.0 [19]	3.8 [49]
$BiVO_4$[a]	2.8	2.3	2.8 [19]	2.9 [50]
$CeVO_4$	1.8	1.0	–	–
Ag_3VO_4	2.2	1.0	0.8	2.2 [14]

[a] These values are for the zircon polymorph of $BiVO_4$.

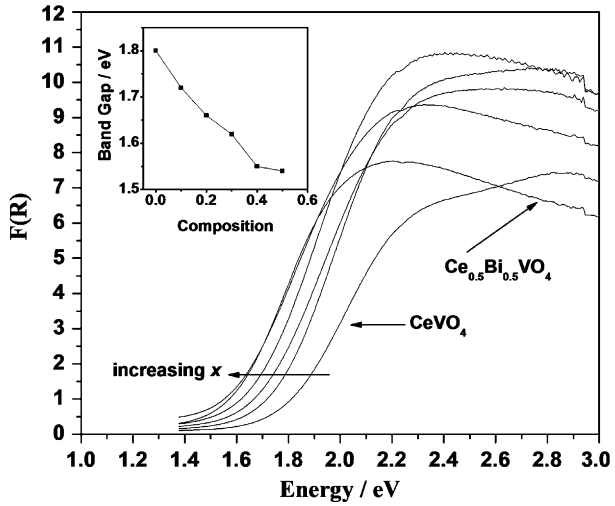

Fig. 2. Diffuse reflectance spectra for $Ce_{1-x}Bi_xVO_4$ solid solution samples for $0<x\leq 0.5$. The inset reveals the relationship between the band gap and the composition of the material.

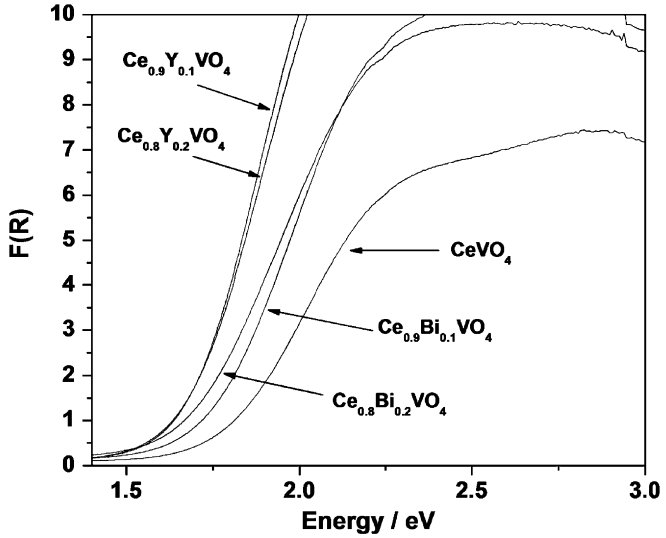

Fig. 3. Diffuse reflectance spectra for phase pure $Ce_{1-x}Y_xVO_4$ and $Ce_{1-x}Bi_xVO_4$ solid solutions.

LUMO is a linear combination of antibonding V 3*d* orbitals and O 2*p* orbitals with *e* symmetry. The SLUMO also originates from antibonding V 3*d*–O 2*p* interactions, but has t_2 symmetry. The LUMO and SLUMO correspond to the expected splitting of *d*-orbitals in a tetrahedral ligand field, calculated here to be 1.3 eV. The HOMO to LUMO excitation corresponds to the so-called ligand-to-metal charge transfer (LMCT) transition. This excitation energy has been reported to be 4.5 eV [35], which is in reasonably good agreement with our calculated value of 4.3 eV.

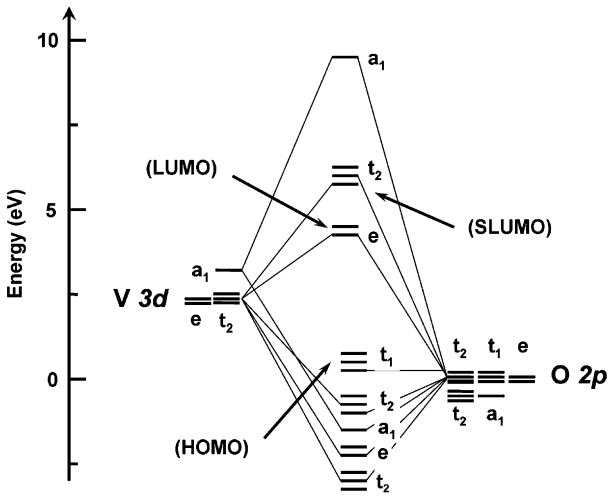

Fig. 4. Molecular orbital diagram of VO_4^{3-} based on the ADF calculations. By convention the HOMO is set at zero energy.

3.4. Band structure calculations

Band gaps derived from LMTO and CASTEP calculations are compared to the experimental band gaps in Table 2. The calculated band gaps are systematically smaller than the experimental values, but they do capture the qualitative trends in the experimental data. At a first glance one might conclude that CASTEP is somewhat more accurate than LMTO in predicting the band gap. On the other hand, if we compare the relative changes in band gap (i.e., YVO_4 to $BiVO_4$) the superiority of one method over the other is not clear cut. Throughout the remainder of this manuscript the band structures obtained with the LMTO code will be reported because of the greater ease with which chemical bonding information can be extracted from the results.

The tendency for DFT calculations in general to underestimate the band gaps of oxides has been previously documented [36–38]. This is due in part to the fact that when using the generalized gradient approximation, the Kohn–Sham eigenvalues do not represent the true quasiparticle energy [39]. Despite this shortcoming the calculations are effective in identifying the orbital interactions that play a key role near the Fermi level.

3.5. Electronic structures of $(Ba)_3(VO_4)_2$ and $Pb_3(VO_4)_2$

When the VO_4^{3-} anion is combined with a cation and condensed into a crystalline solid the energy of the charge transfer

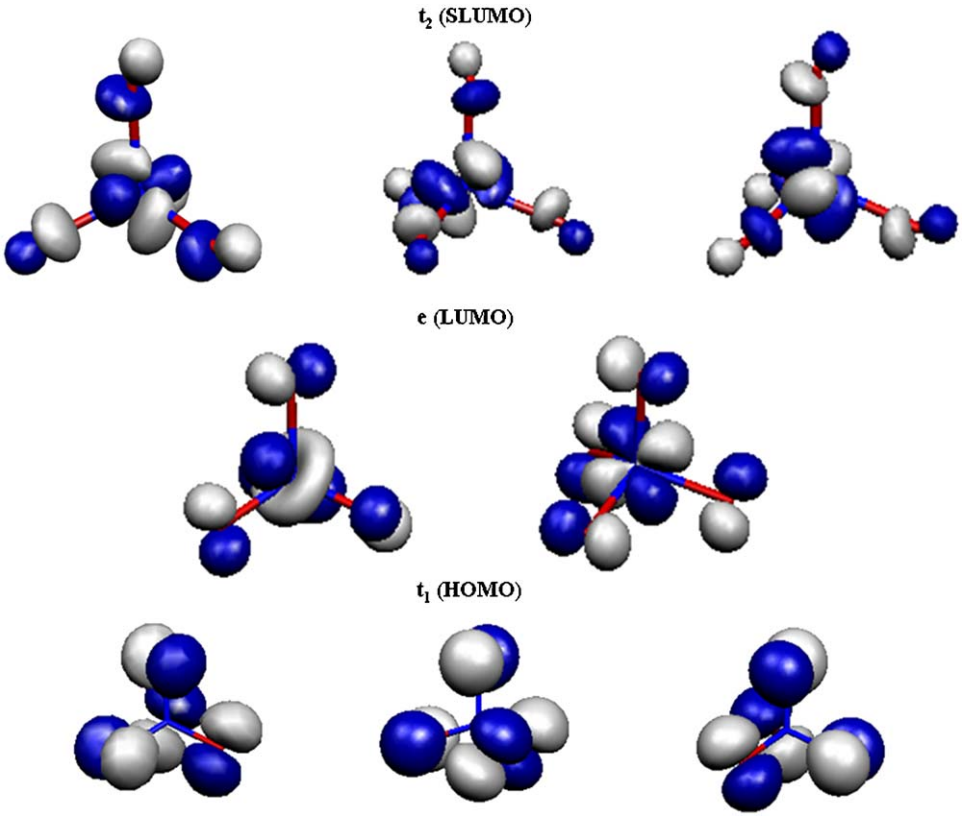

Fig. 5. Orbital interactions of the HOMO, LUMO, and SLUMO in an isolated VO_4^{3-} tetrahedron.

excitation decreases. The magnitude of the decrease depends on the nature of the cation. First consider $Ba_3(VO_4)_2$, where the Ba^{2+}–VO_4^{3-} interaction is largely ionic. The density of states plot for $Ba_3(VO_4)_2$ is shown in Fig. 6.

The electronic structure of $Ba_3(VO_4)_2$ follows directly from the electronic states of the VO_4^{3-} ion. Although the oxygen 2*p* orbitals make the dominant contribution to the valence band, the lower region of the valence band contains a significant V 3*d* contribution. These electronic states originate from the bonding *e* and t_2 orbitals seen in the VO_4^{3-} MO diagram. Upon moving toward the top of the valence band, the V 3*d* contribution decreases as bonding states give way to O 2*p* nonbonding states. The states at the top of the valence band originate from the t_1 orbitals in the VO_4^{3-} MO diagram. The conduction bands arise from the t_2, *e*, and a_1 antibonding orbitals (see Fig. 5) with V 3*d* and O 2*p* orbital character.

From the partial DOS contributions in Fig. 6 we see that the barium orbitals do not play a significant role in the density of states near the band edges. The fact that the vanadate groups are not connected, coupled with the ionic nature of the Ba^{2+}–VO_4^{3-} interaction, leads to the presence of rather flat bands in the band structure diagram (see supplemental information). Nevertheless, the highly concentrated arrangement of VO_4^{3-} groups produces bands that although narrow have a small amount of dispersion. This effect, together with the high concentration of vanadate ions in a salt, is responsible for reducing the charge transfer energy (band gap) from 4.5 eV for an isolated VO_4^{3-} ion to 3.8 eV for $Ba_3(VO_4)_2$.

The density of states plot for $Pb_3(VO_4)_2$, which has a distorted $Ba_3(VO_4)_2$ structure, shows both similarities and differences with respect to $Ba_3(VO_4)_2$. First of all notice that that lead makes a larger contribution than barium, both to the valence and to the conduction bands. Unlike vanadium, the Pb 6*s* and 6*p* orbitals contribute rather evenly across the entire valence band region (0 to −5 eV). Orbital specific PDOS plots (not shown) reveal that the Pb 6*p* orbital contribution is larger at the bottom of the valence band, while the Pb 6*s* orbitals make a larger contribution near the top of the valence band. The Pb 6*p* orbitals make up nearly all of the lead contribution to the conduction band.

The bands that are split off to lower energy (−6 to −8 eV) are predominantly Pb 6*s* nonbonding states. However, there is some mixing with O 2*p* orbitals, via weakly bonding Pb 6*s*–O 2*p* interactions. The corresponding Pb 6*s*–O 2*p* antibonding interactions are found at the top of the valence band. Through this interaction the filled Pb 6*s* orbitals act to destabilize nonbonding O 2*p* states of the vanadate group leading to a reduction of the band gap energy. At the same time the Pb 6*p* orbitals interact with the V 3*d* and O 2*p* orbitals at the bottom of the conduction band, leading to a stabilization of the conduction band, thereby lowering its energy. The net effect is a decrease of 0.7–0.9 eV in the band gap, which is observed both experimentally and computationally, upon moving from $Ba_3(VO_4)_2$ to $Pb_3(VO_4)_2$.

3.6. Electronic structures of YVO_4 and $BiVO_4$

The band structures of the isostructural compounds YVO_4 and $BiVO_4$, as calculated with the CASTEP code, have previously been reported [19]. The LMTO calculated band structures are similar. They are given here (Fig. 7) because they more accurately capture the experimentally observed decrease in band gap (1.0 eV) on going from YVO_4 to $BiVO_4$. The electronic structure of YVO_4 is similar to $Ba_3(VO_4)_2$. Bands originating from V 3*d* and O 2*p* bonding orbitals occupy the lower portion of the valence band

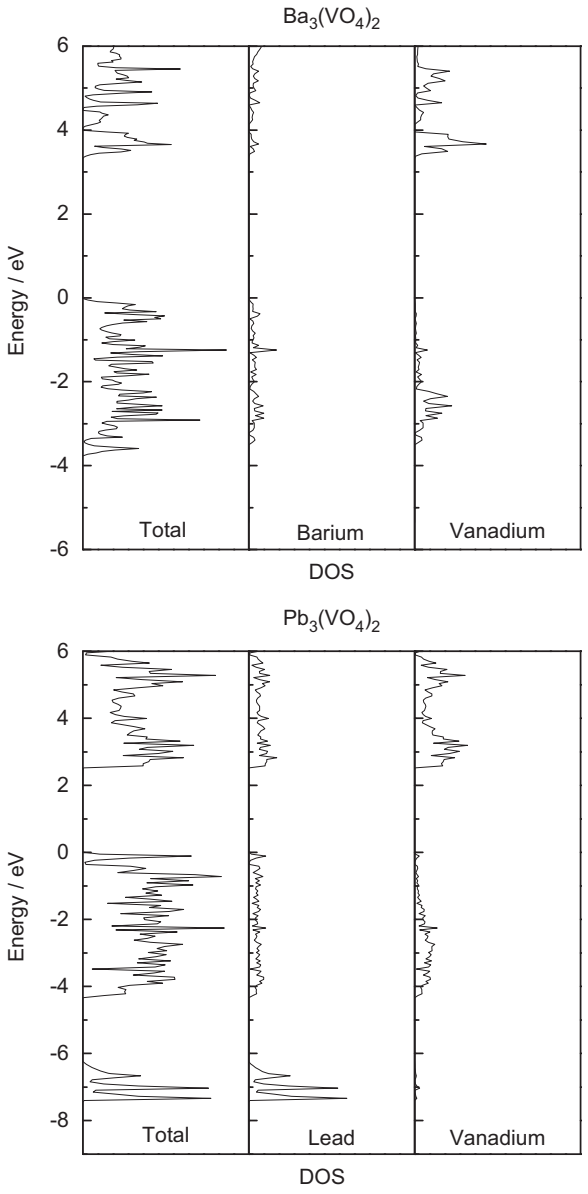

Fig. 6. Density of states (DOS) plots for $Ba_3(VO_4)_2$ (top) and $Pb_3(VO_4)_2$ (bottom). The Fermi level is set to zero energy. The partial density of states (PDOS) contributions of the metal cations are shown to the right. The *x*-axis scale is the same for DOS and PDOS plots.

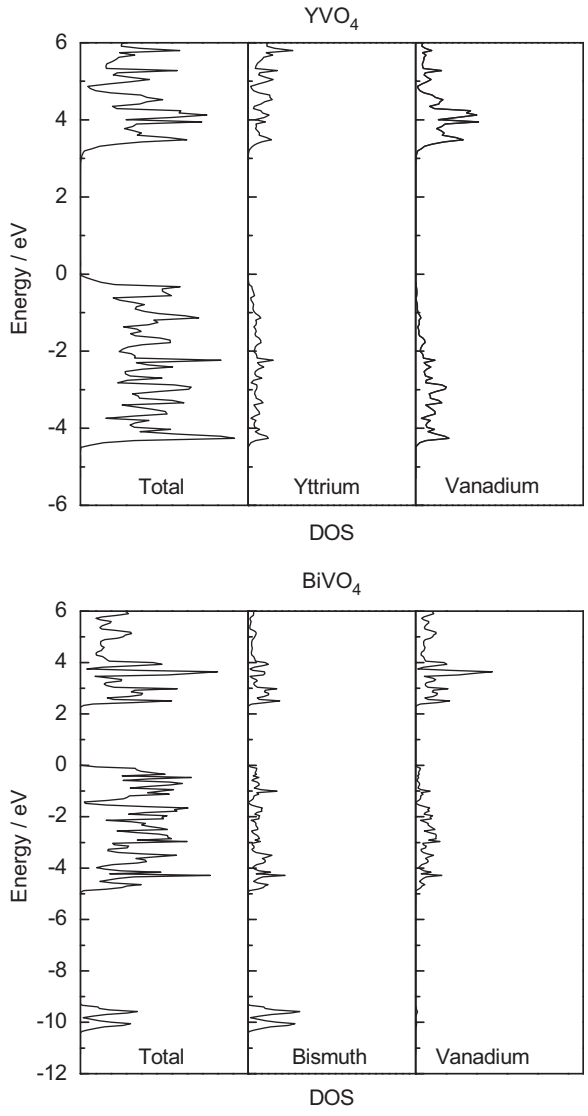

Fig. 7. Density of states (DOS) plots for YVO_4 (top) and $BiVO_4$ (bottom) with the zircon structure. The Fermi level is located at zero energy. The partial density of states (PDOS) contributions of the metal cations are shown to the right. The *x*-axis scale is the same for DOS and PDOS plots.

while the upper portion of the valence band originates from nonbonding O 2*p* states. The conduction band is composed of V 3*d*–O 2*p* antibonding interactions. The bands are quite narrow for reasons similar to $Ba_3(VO_4)_2$ (see supplemental information for *E* vs. *k* plots).

Upon replacing Y^{3+} with Bi^{3+} the basic features of the YVO_4 electronic structure are retained, but additional bands arise that can be attributed to the Bi 6*s* and 6*p* orbitals. The isolated bands located between −9 and −11 eV are mainly Bi 6*s* in character, with a small contribution of the O 2*p* orbitals. These are analogous to the Pb 6*s* "nonbonding" bands in $Pb_3(VO_4)_2$. The Bi 6*s* orbitals are shifted to lower energy (by ~3 eV) with respect to the Pb 6*s* orbitals due to the increase in effective nuclear charge. This alters the energy level matching with the MOs of the vanadate group. As a consequence the Bi 6*s* orbitals appear to hybridize less effectively with the nonbonding MOs of the vanadate group. At the same time the Bi 6*p* orbitals hybridize more effectively with the antibonding orbitals of the VO_4^{3-} group. The net effect is roughly the same, a significant reduction in the band gap (with respect to YVO_4).

3.7. Electronic structure of $CeVO_4$

The band structure of $CeVO_4$ is complicated by the presence of partially filled 4*f* orbitals. Accurately calculating the contributions of 4*f* orbitals to the band structures of lanthanide compounds remains a challenge [40,41]. It is generally accepted that LMTO calculations cannot reliably determine the energies of the 4*f* states [42]. Therefore, we have calculated the band structure of $LaVO_4$ (in its high temperature zircon form) to approximate the band structure of $CeVO_4$. Given their positions in the periodic table it is reasonable to assume that apart from the presence of the $4f^1$ levels the electronic structures of La^{3+} analogs of Ce^{3+} compounds are generally quite similar. Previous studies support this assumption [42].

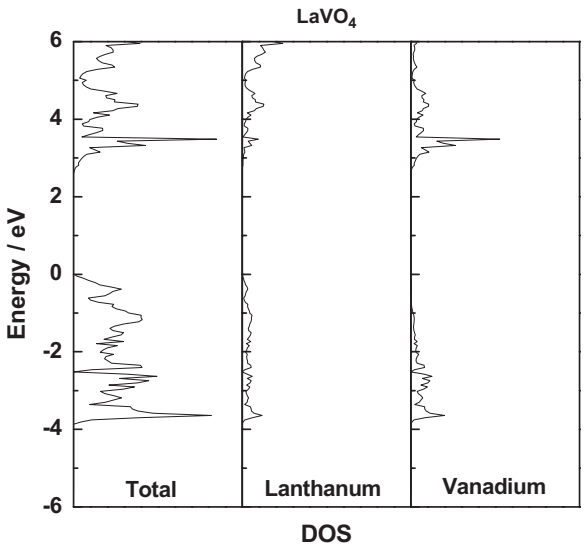

Fig. 8. Density of states (DOS) plots for $LaVO_4$ with the zircon structure. The Fermi level is located at zero energy. The partial density of states (PDOS) contributions of the metal cations are shown to the right. The *x*-axis scale is the same for DOS and PDOS plots.

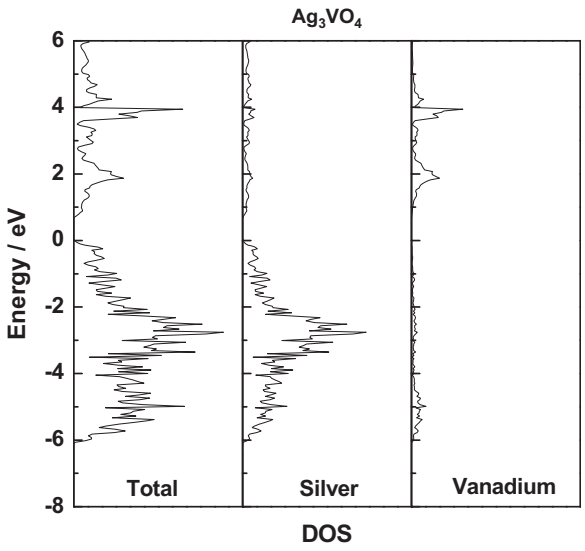

Fig. 9. Density of states (DOS) plots for Ag_3VO_4. The Fermi level is located at zero energy. The partial density of states (PDOS) contributions of the metal cations are shown to the right. The *x*-axis scale is the same for DOS and PDOS plots.

The electronic DOS plot for $LaVO_4$ is shown in Fig. 8. It is similar to the other vanadate salts of cations with a noble gas electron configuration, YVO_4 and $Ba_3(VO_4)_2$. The valence band is composed mainly of O 2*p* and V 3*d* orbitals, while the conduction band is predominantly made up of O 2*p* and V 3*d* antibonding orbitals. There is some hybridization of La 5*d* orbitals with the antibonding conduction band states. We will return to this point later. The calculated band gap of $LaVO_4$ is 2.8 eV, which is 0.2 eV smaller than the calculated band gap of YVO_4 (3.0 eV). Experimentally $LaVO_4$ is reported to have a band gap (3.5 eV) that is 0.3 eV smaller than YVO_4 [43].

The presence of 4*f* levels between the valence and conduction bands differentiates the electronic structure of $CeVO_4$ from those of $LaVO_4$ and YVO_4. Their presence allows for lower energy electronic excitations that are responsible for the dark color of $CeVO_4$. In principle these excitations could involve either (a) transfer of an electron from the nonbonding O 2*p* states that make up the valence band into an unfilled Ce 4*f* orbital or (b) a transfer from the filled 4*f* orbital on Ce^{3+} into the antibonding states that make up the conduction band. In practice, the former excitation is not observed (at least not in the visible region) because the energy needed to add a second electron to the Ce^{3+} site (the Hubbard energy) is large. It is estimated to be ~6 eV [42]. Therefore, the colors of Ce^{3+} compounds are dictated by the energies of the 4*f*–5*d* excitation. While the energy of the Ce 4*f* orbitals is rather insensitive to its surroundings, the energy levels of the 5*d* orbitals can be modified by ligand field effects. Salts where oxygen surround Ce^{3+}, such as $Ce_2(SO_4)_3$, $Ce_2(CO_3)_3$, $Ce(OH)_3$, and $CePO_4$, are generally white, because the 4*f*–5*d* excitation lies in the UV region of the spectrum.

$CePO_4$ is perhaps the best analog to $CeVO_4$. The intrasite 4*f*–5*d* transition in $CePO_4$ peaks at ~4.3 eV (290 nm) with a tail that extends to ~3.1 eV (400 nm) [44]. In $CeVO_4$ the absorption rises sharply above 1.8 eV (690 nm) peaking near ~2.8 eV (440 nm) (see Fig. 1). Depending on what portion of the spectrum we use as a point of reference the 4*f*–5*d* transition is lowered by 1.3–1.5 eV in $CeVO_4$. Hybridization between the Ce 5*d* orbitals and the relatively low lying V 3*d*–O 2*p* antibonding orbitals of the VO_4^{3-} ion is responsible for the small band gap of $CeVO_4$. In a loose sense these excitations could be referred to as Ce 4*f*–V 3*d* charge transfer excitations. In the $CeVO_4$ spectrum one can also see two peaks at ~3.9 and ~4.7 eV just as in $Ba_3(VO_4)_2$. These presumably correspond to expected oxygen-to-vanadium LMCT excitations within vanadate ion ($t_1 \rightarrow e$ and $t_1 \rightarrow t_2$, see Figs. 4 and 5).

The experimental band gap for $CeVO_4$ is measured to be 1.8 eV. If we assume that the energy separation between the valence and conduction bands in $LaVO_4$ and $CeVO_4$ is similar, and use the experimental band gap of 3.5 eV in $LaVO_4$, we can conclude that the Ce 4*f* states are located near the midpoint of the band gap.

3.8. Electronic structure of Ag_3VO_4

By introducing Ag^+, which has a $d^{10}s^0$ electron configuration, a dramatic decrease in the band gap can be realized, with respect to compounds like $Ba_3(VO_4)_2$ and YVO_4. The DOS plot of Ag_3VO_4 is shown in Fig. 9. The most striking feature is the contribution of the Ag 4*d* orbitals across the entire valence band. These states represent both the bonding and antibonding Ag 4*d*–O 2*p* interactions. This interaction destabilizes the electronic states found near the top of the valence band, which directly leads to the observed decrease in the band gap.

3.9. $Ce_{1-x}Bi_xVO_4$ and $Ce_{1-x}Y_xVO_4$ solid solutions

The energies of valence and conduction band edges are often manipulated by making solid solutions between end members. This is the basic principle of semiconductor band gap engineering, where the band gap typically varies smoothly from one end member to the other. In this study solid solutions between $BiVO_4$ and $CeVO_4$ as well as $CeVO_4$ and YVO_4 were explored.

In $Ce_{1-x}Bi_xVO_4$ system the similarities between Ce^{3+} (1.14 Å) and Bi^{3+} (1.17 Å) suggest that a considerable solid solubility should be observed. Experimentally, $BiVO_4$ was found to be soluble in $CeVO_4$ for $0<x<0.5$. All solid solution samples retained the tetragonal zircon structure. Preparation of bismuth rich compositions ($x = 0.6, 0.7, 0.8, 0.9$) resulted in a two phase mixture of phases with nominal compositions of $Ce_{0.5}Bi_{0.5}VO_4$, with the zircon structure, and $BiVO_4$, with the fergusonite structure.

At first glance it is surprising that $Ce_{1-x}Bi_xVO_4$ samples have smaller band gaps than either end member (see Fig. 2). However, given the highly localized nature of the Ce 4*f* orbitals this result is perhaps not so surprising. Assuming that the energy levels of the Ce 4*f* orbitals do not change with composition, the observed trend implies that the energy of the conduction band decreases slightly as Bi^{3+} is introduced. This could be due to symmetry mixing of Bi 6*p* orbitals with the antibonding V 3*d*–O 2*p* bands at the bottom of the conduction band, as seen in $BiVO_4$.

To further investigate this trend, solid solutions of $Ce_{1-x}Y_xVO_4$ were synthesized and diffuse reflectance measurements were performed. Although both end members have the zircon structure, the relatively large size mismatch between Y (1.02 Å) and Ce (1.14 Å) limits the solid solubility range to *x* values near those of the end members. Surprisingly the band gap of $CeVO_4$ decreases when Ce^{3+} is replaced by Y^{3+}, much like it does when Ce^{3+} is replaced by Bi^{3+}. The explanation for this effect is not clear. However, in the bigger picture we can say that the decreases in band gap that occur upon substituting either Bi^{3+} or Y^{3+} into $CeVO_4$ are relatively small. The observed behavior implies that neither the energy levels of the Ce 4*f* states nor the antibonding V 3*d*–O 2*p*–Ce 5*d* states at the bottom of the conduction band are very sensitive to these substitutions.

4. Conclusion

The electronic structures of ternary metal oxides containing the vanadate group have been explored. The electronic structures of $Ba_3(VO_4)_2$ and YVO_4 can be directly interpreted from the VO_4^{3-} molecular orbital diagram as the Ba^{2+} and Y^{3+} cations make a negligible contribution to the electronic structure near the Fermi level. In contrast, the cation orbitals have a considerable impact on the positions of the valence and conduction band edges in those compounds where the cation does not have a noble gas electron configuration. For example, when Ba^{2+} is replaced by Pb^{2+}, the filled Pb 6*s* orbitals raise the top of the valence band while the Pb 6*p* orbitals lower the bottom of the conduction band, resulting in a 0.9 eV reduction in the band gap. A similar effect is seen when Bi^{3+} replaces the Y^{3+} ion in YVO_4.

The band gap of Ag_3VO_4 is smaller than either $Pb_2(VO_4)_2$ or $BiVO_4$ as a consequence of interactions between the Ag 4*d* and O 2*p* orbitals. These interactions destabilize the valence band, raising its energy. When Ce^{3+} is used as a cation, an even more dramatic change takes place as a result of excitations from partially filled *f* orbitals into the conduction band states. The conduction band is formed largely from antibonding orbitals of the vanadate ions, with some Ce 4*d* character. The band gaps of solid solutions involving $CeVO_4$, namely $Ce_{1-x}Bi_xVO_4$ and $Ce_{1-x}Y_xVO_4$, do not vary linearly between end members. Instead the band edges sharpen and decrease subtly from the band gap of pure $CeVO_4$. These compositions have band gaps that are determined by the relative energies of the Ce 4*f* orbitals and the conduction band edge.

Acknowledgments

The initial studies that inspired this work were carried out by students in Chemistry 123 at Ohio State University during the spring quarters of 2006 and 2007. This work was made possible by the support of the National Science Foundation (CHE-0532250) for the Ohio Research Experiences Enhance Learning (REEL) program.

Appendix A. Supplementary material

Supplementary data associated with this article can be found in the online version at doi:10.1016/j.jssc.2009.04.032.

References

[1] A. Hladnik, T. Muck, Dyes Pigm. 54 (2002) 253–263.
[2] N. Imanaka, T. Masui, T. Itaya, Chem. Lett. 32 (2003) 400–401.
[3] M. Jansen, H.P. Letschert, Nature 404 (2000) 980–982.
[4] P.P. Rao, M.L.P. Reddy, Dyes Pigm. 63 (2004) 169–174.
[5] P.P. Rao, M.L.P. Reddy, Dyes Pigm. 73 (2006) 292–297.
[6] R.D. Harley, Artists' Pigments c. 1600–1835: A Study in English Documentary Sources, Butterworth Scientific, London, 1982.
[7] R.D. Kumar, G.Wilker, in: Proceedings of the Eighty Second Annual Meeting Program of the FSCT, 2004, pp. 29/13–29/21.
[8] W. Winter, Pitture e Vernici, European Coatings 79 (2003) 19–24.
[9] P. Wood, F.P. Glasser, Ceram. Int. 30 (2004) 875–882.
[10] M. Oshikiri, M. Borero, J. Ye, Z. Zou, G. Kido, J. Chem. Phys. 117 (2002) 7313–7318.
[11] W. Yao, J. Ye, J. Phys. Chem. B 110 (2006) 11188–11195.
[12] J. Ye, Z. Zou, M. Oshikiri, A. Matsushita, A. Shimoda, M. Imai, M. Shishido, Chem. Phys. Lett. 356 (2002) 221–226.
[13] X. Hu, C. Hu, J. Solid State Chem. 180 (2007) 725–732.
[14] R. Konta, H. Kato, H. Kobayashi, A. Kudo, Phys. Chem. Chem. Phys. 5 (2003) 3061–3065.
[15] H. Honda, A. Ishizaki, R. Soma, K. Hashimoto, A.J. Fujishima, Illum. Eng. Soc. 27 (1998) 42–49.
[16] K. Kobayakawa, C. Sato, Y. Sato, A. Fujishima, J. Photochem. Photobiol. A 118 (1998) 65–69.
[17] A. Fujishima, K. Honda, Nature 238 (1972) 37–38.
[18] Z. Zou, J. Ye, K. Sayama, H. Arakawa, Nature 414 (2001) 625–627.
[19] M.W. Stoltzfus, P.M. Woodward, R. Seshadri, J.-H. Klepeis, B. Bursten, Inorg. Chem. 46 (2007) 3839–3850.
[20] P. Kubelka, F. Munk, Z. Tech. Phys. 12 (1931) 593.
[21] I.P. Shapiro, Opt. i Spektrosk. 4 (1958) 256–260.
[22] O.K. Andersen, Phys. Rev. B 12 (1975) 3060–3083.
[23] O.K. Andersen, O. Jepsen, Phys. Rev. Lett. 53 (1984) 2571–2574.
[24] J.P. Perdew, W. Yue, Phys. Rev. B 33 (1986) 8800–8802.
[25] W. Milman, B. Winkler, J.A. White, C.J. Pickard, M.C. Payne, E.V. Akhmatskaya, R.H. Nobes, Int. J. Quantum Chem. 77 (2000) 895–910.
[26] J.P. Perdew, J.A. Chevary, S.H. Vosko, K.A. Jackson, M.R. Pederson, D.J. Singh, C. Fiolhais, Phys. Rev. B 46 (1992) 6671–6687.
[27] G. TeVelde, E.J. Baerends, J. Comp. Phys. 99 (1992) 84–98.
[28] A. Durif, Acta Crystallogr. 12 (1959) 420–421.
[29] A. Grzechnik, P.F. McMillan, J. Solid State Chem. 132 (1997) 156–162.
[30] P. Tarte, J. Thelen, Spectrochim. Acta A 28 (1972) 5–14.
[31] H. Kasatani, T. Umeki, H. Terauchi, J. Phys. Soc. Jpn. 61 (1992) 2309–2316.
[32] B.G. Hyde, S. Andersson, Inorganic Crystal Structures, Wiley, New York, 1989.
[33] T.A. Albrecht, C.L. Stern, K.R. Poeppelmeier, Inorg. Chem. 46 (2007) 1704–1708.
[34] A. Watanabe, J. Solid State Chem. 153 (2000) 174–179.
[35] A.C. Stuckl, C.A. Daul, H.U. Gudel, J. Chem. Phys. 107 (1997) 4606–4617.
[36] H.W. Eng, P.W. Barnes, B.M. Auer, P.M. Woodward, J. Solid State Chem. 175 (2003) 94–109.
[37] H. Mizoguchi, H.W. Eng, P.M. Woodward, Inorg. Chem. 43 (2004) 1667–1680.
[38] H. Mizoguchi, P.M. Woodward, Chem. Mater. 16 (2004) 5233–5248.
[39] W.R. Lambrecht, Phys. Rev. B 62 (2000) 13538–13545.
[40] S. Fabris, S. de Gironcoli, S. Baroni, G. Vicario, G. Balduci, Phys. Rev. B 71 (2005) 041102.
[41] G. Kresse, P. Blaha, J.L.F. da Silva, M.V. Ganduglia-Pirovano, Phys. Rev. B 72 (2005) 237101.
[42] G. Gauthier, S. Jobic, F. Boucher, P. Macaudire, D. Huguenin, J. Rouxel, R. Brec, Chem. Mater. 10 (1998) 2341–2347.
[43] P. Parhi, V. Manivannan, Solid State Sci. 10 (2008) 1012–1019.
[44] T. Masui, H. Tategaki, S. Furukawa, N. Imanaka, J. Ceram. Soc. Jpn. 112 (2004) 646–649.
[45] P. Suesse, M.J. Buerger, Z. Kristallogr. Kristallgeom. Kristallphy. Kristallchem. 131 (1970) 161–174.
[46] P. Garnier, G. Calvarin, J.F. Berar, D. Weigel, Mater. Res. Bull. 19 (1984) 407–414.
[47] W.O. Milligan, L.W. Vernon, J. Phys. Chem. 56 (1952) 145–148.
[48] A.W. Sleight, A. Ferretti, H.Y. Chen, D.E. Cox, Mater. Res. Bull. 14 (1979) 1571–1581.
[49] A. Jayaraman, G.A. Kourouklis, G.P. Espinosa, A.S. Cooper, L.G. Van Uitert, J. Phys. Chem. Solids 48 (1987) 755–759.
[50] S. Tokunaga, H. Kato, A. Kudo, A. Chem. Mater. 13 (2001) 4624–4628.